RESEARCH Open Access



Enhanced engraftment and immunomodulatory effects of integrin alpha-2-overexpressing mesenchymal stromal cells in lipopolysaccharide-induced acute lung injury

Hana Kang¹, Ok-Hyeon Kim², Eun Seo Chang¹, Jinho Kim³, Ji-Young Kim³, Geun-Seup Shin³, Chul-Hong Kim³, Younghyun Lim³, Young-Jin Seo³, Jung-Woong Kim^{3*} and Hyun Jung Lee^{1,2*}

Abstract

Background Human mesenchymal stromal cells (MSCs) have potential as a treatment for inflammatory diseases, including acute lung injury (ALI), due to their anti-inflammatory and immunomodulatory properties. However, their clinical efficacy is often limited by poor post-transplant survival and adaptability in the host environment. Accordingly, MSCs are primed to boost their therapeutic efficacy for treating a variety of diseases. In our previous study, we discovered that culturing MSCs in a functional polymer-based 3D niche, which simulates the in vivo microenvironment, significantly increased integrin alpha 2 (ITGA2) expression compared to traditional 2D cultures, as revealed by RNA-seq analysis.

Methods ITGA2 was used to prime MSCs and their therapeutic potential evaluated in ALI models. Human bone marrow-derived MSCs were transfected with mEmerald-ITGA2 vectors and intravenously injected at 6 h post-ALI induction. Histological and biochemical analyses explored the therapeutic effects and molecular mechanisms of ITGA2-MSCs (ITGA2 overexpressing MSCs) in lipopolysaccharide (LPS)-induced ALI models.

Results ITGA2-MSCs effectively ameliorated lung tissue injury and lowered blood IL-6 levels compared to that of the control group. Additionally, CD206 expression was highest in the ITGA2-MSC group, which was associated with the activation of M2 macrophage polarization, which contributed to inflammation reduction and tissue repair. Finally, ITGA2-MSCs demonstrated enhanced survival and adaptability when intravenously administered to mice, as indicated by the in vivo imaging system (IVIS).

Conclusions ITGA2 creates a favorable microenvironment for MSCs, enhancing their immunomodulatory functions, ultimately offering a promising strategy for MSC-based cell therapy for ALI.

*Correspondence: Jung-Woong Kim jungkim@cau.ac.kr Hyun Jung Lee pluto38@cau.ac.kr

Full list of author information is available at the end of the article



© The Author(s) 2025. **Open Access** This article is licensed under a Creative Commons Attribution-NonCommercial-NoDerivatives 4.0 International License, which permits any non-commercial use, sharing, distribution and reproduction in any medium or format, as long as you give appropriate credit to the original author(s) and the source, provide a link to the Creative Commons licence, and indicate if you modified the licensed material. You do not have permission under this licence to share adapted material derived from this article or parts of it. The images or other third party material in this article are included in the article's Creative Commons licence, unless indicated otherwise in a credit line to the material. If material is not included in the article's Creative Commons licence and your intended use is not permitted by statutory regulation or exceeds the permitted use, you will need to obtain permission directly from the copyright holder. To view a copy of this licence, visit http://creativecommons.org/licenses/by-nc-nd/4.0/.

Keywords Acute lung injury (ALI), Integrin alpha 2 (ITGA2), Mesenchymal stromal cells (MSCs), Immunomodulation, Cell therapy

Background

Acute lung injury (ALI) and its severe form, acute respiratory distress syndrome (ARDS), are life-threatening inflammatory conditions characterized by diffuse damage to the pulmonary capillary endothelium and alveolar epithelium. These conditions can arise from various triggers, including infection, shock, and blood transfusion [1]. Recently, the ALI/ARDS incidence has increased significantly, largely due to the coronavirus disease 2019 (COVID-19) pandemic. Notably, approximately 33% of patients with COVID-19 developed ALI/ARDS, with respiratory failure accounting for 53% of ARDS-related deaths [2, 3]. Even beyond the pandemic, ALI/ARDS remains a critical healthcare challenge, exhibiting high morbidity and mortality rates. A large multicenter prospective cohort study reported that 10.4% of intensive care unit (ICU) admissions met the criteria for ALI/ ARDS, with a mortality rate of 46.1% among patients with severe ARDS [4].

Beyond the acute phase, ARDS survivors experience considerable long-term complications that contribute to elevated mortality and reduced quality of life. These morbidities include cognitive and psychological impairments, diminished exercise capacity due to muscle wasting, pulmonary function deficits, and persistent healthcare dependence [5–7]. Notably, these post-ARDS sequelae result in a heightened risk of mortality, particularly within the first year.

Given the pressing need for effective interventions, cell-based therapies have been extensively explored for ALI/ARDS over the past few decades [8, 9]. Preclinical studies have demonstrated the therapeutic potential of various cell types, including circulating endothelial progenitor [10] and alveolar type II cells [11]. Among these, mesenchymal stromal cells (MSCs) have garnered particular attention due to their potent immunomodulatory and regenerative properties [12–15]. MSCs mitigate endotoxin- and *Escherichia coli*-induced lung injury, partly through the secretion of growth factors, such as keratinocyte growth factor and anti-inflammatory cytokines, such as IL-10 [16, 17].

Despite their promising applications, the clinical translation of MSC therapy for ARDS remains limited. Although over 100 clinical trials have investigated MSC-based therapies for various conditions, only a small number have specifically targeted ARDS. A prospective, double-blind, multicenter randomized trial demonstrated that MSC administration significantly reduced plasma levels of angiopoietin-2 and C-reactive protein in ARDS patients compared to controls [18]. Similarly, Bellingan

et al. reported that MSC therapy reduced mortality and increased ventilator- and intensive care unit (ICU)-free days compared to the placebo [19]. However, conflicting results exist; for instance, while one study found that allogeneic adipose-derived MSCs (AD-MSCs) improved the oxygenation index in ARDS patients, they did not significantly impact ventilator- or ICU-free days or levels of inflammatory cytokines IL-6 and IL-8 [20]. A critical limitation in MSC therapy is the suboptimal survival and homing efficiency of transplanted cells, which hampers their sustained therapeutic efficacy [21]. To overcome these challenges, transplanted cells must achieve prolonged retention, enhanced in vivo survival, and potentiated functionality. Previous studies have demonstrated that integrins on MSCs contribute to lung entrapment and retention, with avb3 integrin in particular playing a critical role in mediating binding to the vascular endothelium. Additionally, the integrin complex containing ITGA2 (a2b1) expressed on endothelial cells [22] or smooth muscle cells [23] has been reported to significantly enhance cellular adhesion in vivo. These findings suggest that modulating adhesion molecules on MSCs may represent a promising strategy to enhance MSC adhesion, engraftment, and therapeutic efficacy in the context of lung injury [24].

In our previous study, we aimed to enhance the immunomodulatory and anti-inflammatory properties of MSCs by culturing them in a three-dimensional (3D) matrix that mimics the native stem cell niche [25]. However, the underlying mechanisms responsible for these enhanced effects remained unclear. To further investigate these mechanisms, we performed RNA sequencing (RNA-seq) analysis and identified adhesion molecules, such as integrin alpha 2 (ITGA2), as potential contributors.

Given that various priming strategies have been employed to improve the therapeutic efficacy of MSCs, we focused on modulating ITGA2 expression to optimize MSC function. In this study, we examined the therapeutic potential and engraftment efficiency of ITGA2-modulated MSCs (ITGA2-MSCs) in a mouse model of acute lung injury (ALI). Our work aims to provide new insights into MSC-based therapeutic strategies for ALI/ARDS and inform future translational and clinical applications.

Methods

Cell culture

Human bone marrow MSCs were derived from whole bone marrow from independent human donors (commercially available by AllCells, Alameda, CA, USA). Cells were cultured in Minimal Essential Medium alpha (MEM-α, Cytiva HyClone, Marlborough, MA, USA) supplemented with 20% fetal bovine serum (FBS, GW Vitek, Geumcheon-gu, Seoul, Korea), and 1% penicillin/streptomycin (Thermo Fisher Scientific, Waltham, MA, USA) in a humidified atmosphere of 5% CO₂ at 37 °C. The human monocyte cell line THP-1 [26] was purchased from the Korean Cell Line Bank (KCLB, Jongno-gu, Seoul, Korea) and maintained in Roswell Park Memorial Institute medium (RPMI) 1640 medium (Welgene, Gyeongsan-si, Gyeongsangbuk-do, Korea) supplemented with 10% FBS (GW Vitek), 1% penicillin/streptomycin (Thermo Fisher Scientific), and 0.05 mM 2-mercaptoethanol (Sigma-Aldrich, St. Louis, MO, USA). All cells were incubated at 37 °C in a humidified incubator with 5% CO₂. All cell lines were routinely tested for mycoplasma contamination.

RNA sequencing and library preparation

RNA-seq libraries were prepared using the TreSeq mRNA Library Prep Kit (Illumina, USA) following the manufacturer's instructions. Briefly, 100 ng of total RNA was reverse-transcribed using oligo-dT primers, followed by second-strand cDNA synthesis. Double-stranded cDNA was purified using AMPure XP beads (Beckman Coulter, USA), and adapter were ligated before library amplification, Final libraries were sequenced on the NovaSeq 600 platform (Illumnia, USA) to generate 101-bp paired-end reads.

RNA-seq data processing and bioinformatical analysis

The variations in gene expression between MSCs cultured in a 2D and 3D environment, transcriptome analysis was performed using mRNA sequencing. Raw sequence reads were trimmed to remove adaptor sequence and masked for low-quality sequences using TrimGalore (ver. 0.6.6). Processed reads were aligned to Homo Sapiens transcriptome annotation (GRCh38.p13.103) using STAR (ver. 2.7.1a). The count values of transcripts were estimated by RSEM (ver. 1.3.3). The FPKM values were calculated using the 'fpkm' function from DESeq2 (ver. 1.32.0) that operates on the robust median ratio method. To analyze the transcripts as DE (differential expression), DESeq2 (ver. 1.32.0) calculates results based on the normalized counts from entire sequence counts with R (ver. 4.1). Transcripts were considered significantly differentially expressed if they met the following criteria: absolute log 2 fold change > 1, p-value < 0.05 across all experimental comparisons. All data analysis and visualization was performed using matplotlib (ver. 3.5.1) and seaborn (ver. 0.11.2) with Python (ver. 3.7).

Ectopic integrin alpha 2 (ITGA2) expression

To ensure 60–70% confluence for transfection the following day, MSCs were seeded at a density of 4×10^4 cells per well in a six-well plate. The mEmerald-integrin-alpha-2

or mEmerald-N1 construct (Addgene, Massachusetts, Watertown, USA) was mixed with FuGENE6 (Promega, Madison, WI, USA) in Opti MEM medium (Thermo Fisher Scientific). After 20 min of incubation at room temperature, the mixture was added to the cells. Following incubation for 48 h, the efficiency of transfection was confirmed using quantitative real-time polymerase chain reaction (qRT-PCR).

Animals

Male C57BL/6 mice (8-10 weeks old, weight 19-22 g) were purchased from DBL (Eumseong-gun, Chungcheongbuk-do, Korea). In this experimental setup, we used only male mice to induce the ALI model. Five mice were housed per cage under controlled environmental conditions (21 ± 2 °C, 12 h light/dark cycle) and provided a standard laboratory diet and tap water ad libitum. The experimental procedures were approved by the Institutional Animal Care Use Committee (IACUC) of Chung-Ang University (Approval ID:202301020051). In particular, given that the ALI model is associated with variable survival outcomes, a greater number of mice were allocated to the vehicle group to account for potential mortality and to ensure sufficient data acquisition. Mice were randomly divided into four experimental groups: (1) Sham (n = 20), (2) vehicle (n = 38), (3) MSC (n = 30), and (4) ITGA2-MSC (n = 30). ALI was induced in all groups except for the Sham group by intratracheal administration of lipopolysaccharide (LPS; 20 mg/kg, E.coli serotype O111:B4, Sigam-Aldrich) in 100 μL of setrile saline. General anesthesia was induced using 3-5% isoflurane (Hana Pharm Co., Hwaseong, Gyeonggi-do, Korea) delivered in oxygen via inhalation for 5 min and maintained throughout the procedure.

Six hours after LPS administration, mice in the MSC and ITGA2-MSC groups received 1×10^6 cells via tail vein injection. Prior to injection, cells were maintained at 37 °C for 48 h following transfection with either control or ITGA2 plasmid, harvested by trypsinization and suspended in sterile PBS. Each mouse received a total injection volume of 200 μL . The sham and vehicle groups received an equivalent volume of saline without cells. Mice were monitored for survival over an 8-day period. Blood and lung tissues were collected at designated time point for downstream analysis, as illustrated in Fig. 1A. Mice that lost more than 10% of their body weight following the procedure were excluded from further analysis and euthanized using carbon dioxide. The work has been reported in line with the ARRIVE guideline 2.0.

Tumor necrosis factor (TNF)-α suppression assay

Murine splenocytes were isolated from 5-weeks-old ICR mice for co-culture with MSCs. Briefly, the spleen was mechanically dissociated through a 70 μ m strainer to

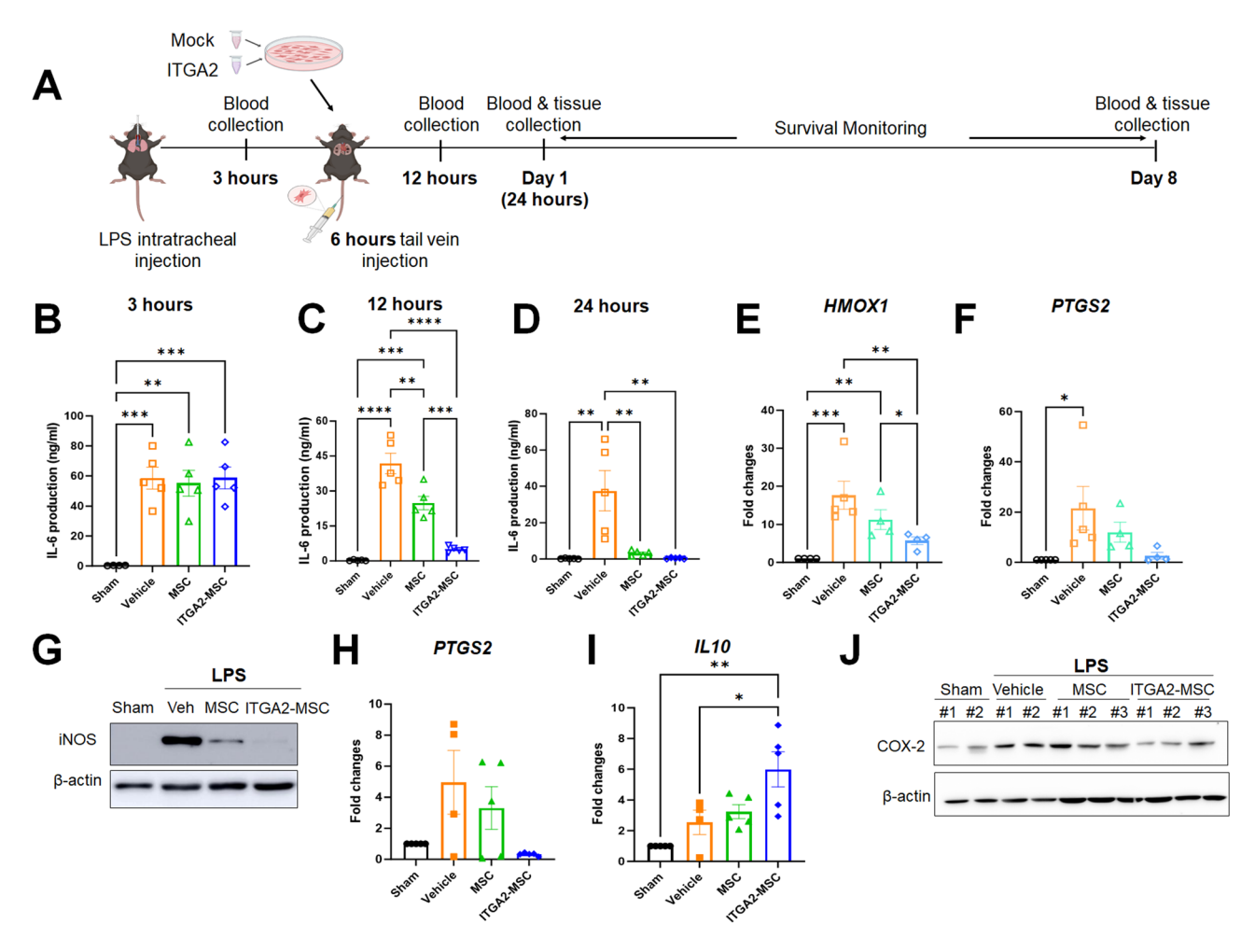


Fig. 1 Enhanced therapeutic effect of ITGA2-MSCs in a mouse LPS-induced ALI model. (**A**) Schematic overview of the ALI model and ITGA2-MSC treatment regimen. Mice were intratracheally injected with 20 mg/kg of LPS, followed by intravenous administration of 10^6 MSCs or ITGA2-MSCs 6 h later. Blood samples were collected at 3, 12, and 24 h, and 8 days post-LPS injection. (**B-D**) ELISA quantification of serum IL-6 levels at 3, 12, and 24 h post-LPS injection in the sham, vehicle, MSC, and ITGA2-MSC groups (n=4-5 per group). (**E**) and (**F**) Transcript levels of *HMOX1* and *PTGS2* in lung tissues 24 h after LPS injection. (**G**) Immunoblot analysis of iNOS protein expression in lung tissues. (**H-J**) Real time quantitative-PCR analysis of *PTGS2* and *IL10* genes, and Immunoblot analysis of COX-2 protein expression in lung tissues 8 days after LPS injection (n=5 per group). Statistical significance was determined using two-way ANOVA. *p < 0.05, **p < 0.01, ****p < 0.001, ****p < 0.001, ****p < 0.001, ****p < 0.001, *****p < 0.0001. The number of animals used in each analysis is as follows: For histological analysis-sham (n=8), vehicle (n=8), MSC (n=12), and ITGA2-MSC (n=8); for IL-6 cytokine analysis-sham (n=4), vehicle (n=5), MSC (n=5), and ITGA2-MSC (n=5). Immunoblot images were cropped and full-length blots are presented in Supplementary Fig. 6

exclude all connective tissue, lysed in Red Blood Cell Lysing Buffer Hybri-Max (Sigma-Aldrich) and resuspended in medium (MEM- α , 20% FBS, 1% P/S) after washing with phosphate-buffered saline (PBS) for culture with MSCs. Splenocyte-MSC co-cultures were plated at a ratio of 30 to 1. LPS (1 µg/mL, Sigma Aldrich) was added 30 min after plating. Following 4 h incubation at 37 °C, the supernatant was collected and analyzed for TNF- α using the CymaxTM Mouse TNF- α ELISA kit (Ab Frontiers, Geumcheon-gu, Seoul, Korea) and interleukin (IL)-10 using the Mouse IL-10 Quantikine ELISA kit (R&D systems, Minneapolis, MN, USA) according to the manufacturer's instructions.

Prostaglandin E₂ (PGE₂) and IL-6 production

PGE₂ production was measured in human bone marrow-derived MSCs transfected with a control or ITGA2 plasmid. After 24 h of incubation at 37 °C, the supernatant was collected and analyzed for PGE₂ using a PGE₂ ELISA kit (R&D Systems Inc., Minneapolis, MN, USA). The concentration of PGE₂ was measured using ELISA kit according to the instructions provided by the manufacturer.

For IL-6, the distal tail of mouse was cut at 3 h, 12 h, and 24 h after ALI, and the blood was drawn into a pipette tip to collect peripheral blood. The samples were centrifuged for 15 min at 3000 rpm and 4 $^{\circ}$ C, and the serum was stored at -80 $^{\circ}$ C for analysis. The IL-6 levels

were measured using ELISA kits (Ab Frontiers) according to the manufacturer's guidelines.

RNA extraction

Total RNA from cultured cells was extracted using the RNeasy Mini Kit (Qiagen, Hilden, North Rhine-Westphalia, Germany) according to the manufacturer's instruction. For lung tissue samples, RNA extraction was performed using TRIzol reagent (Invitrogen, Carlsbad, CA, USA) and homogenized with a disposable Biomasher homogenizer (Nippi, Tokyo Adachi, Japan). After homogenization, 1-bromo-3-chloropropane (BCP; Sigma) was added to the lysate, followed by vigorous inversion and centrifugation to separate the aqueous phase. The resulting supernatant was carefully transferred and mixed with isopropanol by gentle inversion, then centrifuged to precipitate the RNA. The RNA pellet was washed three times with 70% ethanol, air-dried, and dissolved in RNase-free water. RNA concentration and purity were assessed using a UV/VIS Nano spectrophotometer (Nabi, MicroDigital Co., Ltd., Bundang-gu, Seongnam-si, Gyeonggi-do, Korea).

qRT-PCR

The reverse transcription was performed using a Maxima First Strand cDNA Synthesis Kit (Thermo Fisher Scientific). qRT-PCR was performed using the Power SYBR Green PCR Master Mix reagent (Applied Biosystems, Foster city, CA, USA) and QuantStudio3 Real-Time PCR (Applied Biosystems). The relative quantification of target genes was normalized to that of GAPDH, and the $^{2-\Delta\Delta}$ Ct method was used to calculate the gene expression. Expression levels of PTGS2, IDO, HMOX1, PTGES, ITGA2, IL10, OCLN, CLDN2, CLDN4, CD86, CD206, NOS2, and ARG1 were evaluated. The primer sequences used in this study are presented in Supplementary Information.

Immunoblotting

Total protein was extracted from lung tissue samples using radioimmunoprecipitation assay buffer (RIPA) buffer containing 1% protease and phosphatase inhibitor cocktails (Sigma-Aldrich) and a Biomasher (nippi, Tokyo Adachi, Japan) disposable homogenizer. Total protein was quantified using a protein assay dye (Bio-Rad). Protein samples were separated on a 10% sodium dodecyl sulfate-polyacrylamide gel electrophoresis (SDS-PAGE) gel and transferred to a nitrocellulose membrane with a pore size of 0.2 μ m. Membranes were blocked in a blocking buffer containing 5% skim milk in Tris-buffered saline with 0.1% Tween 20 (TBS-T) for 1 h. After blocking, the membranes were incubated overnight at 4 °C with primary antibodies. For immunoblotting, the antibodies used were as follows: anti-cyclooxygenase-2 (COX-2,

1:1000, ab102005, Abcam, Cambridgeshire, Cambridge, UK), anti-Inducible Nitric Oxide Synthase (iNOS, 1:1000, 06-573, Merck KGaA, Hesse, Darmstadt, Germany), and β-actin (1:1000, sc-47778, Santa Cruz Biotechnology, Santa Clara, CA, USA). The membranes were then washed thrice with TBS-T and incubated with secondary antibodies at room temperature for 2 h. Protein band intensities were visualized and analyzed using enhanced chemiluminescence (ECL) immunoblotting reagents (Westar Supernova, Cyanagen, Italy) and Amersham ImageQuant™ 500 biomolecular imager (Cytiva, Massachusetts, Marlborough, USA).

Histological assessment

The left lung lobes were collected from all groups, and lung tissue samples were fixed in 10% neutral buffered formalin (NBF) (BIOSESANG, Seongnam-si, Gyeonggido, Korea). The samples then underwent a sequential dehydration process and were embedded in paraffin blocks. The paraffin-embedded Sect. (4 µm in thickness) were mounted onto glass slides, dried, and subjected to hematoxylin and eosin (H&E) staining. The section was treated with xylene, followed by a series of ethanol solutions with progressively decreasing concentrations, hematoxylin, and eosin, before being mounted according to the manufacturer's instructions. H&E-stained images were obtained from an inverted microscope equipped with a camera (Leica microscope system, Wetzlar, Hesse, Germany) and ALI scoring was performed based on histological changes as previously reported [27].

In vivo imaging system (IVIS)

Mock-MSCs or ITGA2-modulated MSCs (5×10⁵ cells) were stained with 50 µg/mL IVISense 680 Fluorescent Cell Labeling Dye (Perkin Elmer, Massachusetts, Waltham, USA) before injection. The stained cells were incubated for 15 min at room temperature in the dark. After incubation, the cells were washed thrice with PBS containing 1% FBS and resuspended in 200 µL of saline for injection. The prepared cell suspension was administered via tail vein injection into C57BL/6J mice (n=3)per group used for IVIS imaging). Prior to imaging, the dorsal fur of the mice was trimmed, and the animals were anesthetized with 5% isoflurane in oxygen for induction, followed by maintenance at 3% isoflurane. Imaging was performed using an IVIS (VISQUE) (Vieworks, Anyang-si, Gyeonggi-do, Korea) with the mice positioned dorsally. Fluorescence imaging was conducted daily from day 1 to day 7 post-injection using Cy5.5 filters and HyperRed light settings. The software automatically defined the regions of interest (ROI) and applied signal correction. The total fluorescence signal was quantified by summing the radiant efficiency values within each ROI. Fluorescence intensity was measured in units of radiant efficiency ([p/s/cm²/sr]/[μ W/cm²]). To ensure consistency and comparability across the groups, all images were acquired under identical exposure times and imaging conditions.

Immunofluorescence staining

Lung tissues were post-fixed in 10% neutral buffered formalin (BIOSESANG) and embedded in paraffin. Section (5 μm) were cut, incubated at 60 °C for 1 h, and deparaffinized with xylene followed by a graded ethanol series. Antigen retrieval was performed in 10 mM sodium citrate buffer (pH 6.0) at 120 °C for 15 min using a TintoRetriever pressure Cooker (Bio SB, California, Santa Barbara, USA). After cooling for 20 min, the sections were washed with PBS and tissue boundaries were outlined with an oil-pen.

Sections were blocked with 5% BSA and 0.1% Triton X-100 in PBS (0.1% PBS-T) for 1 h at room temperature, followed by overnight incubation with anti-CD206 antibody (1:100, Proteintech, Illinois, Rosemont, USA) in 1% BSA/0.1% PBS-T. After Following three washes with 0.1% PBS-T for 10 min each, the sections were treated with a secondary antibody, Donkey Anti-Rabbit IgG H&L (Alexa Fluor 594; Abcam, Cambridgeshire, Cambridge, UK), diluted 1:400 in 1% BSA/0.1% PBS-T, for 2 h at room temperature. Finally, the sections were washed thrice in 0.1% PBS-T for 10 min each on a shaker. Next, samples were washed with 0.1% PBS-T by shaking for 10 min, thrice. Counter staining was performed with 4',6-diamidino-2-phenylindole (DAPI) (Vector Laboratories Inc., San Francisco, CA, USA) and the slides were prepared using an antifade mounting medium. Fluorescence imaging was performed with an inverted microscope (Eclipse Ti2, Nikon, Tokyo, Minato, Japan).

THP-1 co-culture transcript analysis

THP-1 cells were seeded at a density of 8×10^5 cells per well in 6-well plates and treated with 200 µg/mL phorbol 12-myristate 13-acetate (PMA, MedchemExpress, New Jersey, Monmouth, USA) for 24 h to induce differentiation. Following confirmation of morphological transition from suspension to adherent cells, the medium was removed, and the cells were stimulated with LPS of 10 ng/mL for 48 h. Subsequently, a transwell co-culture system was established wherein MSCs or ITGA2-modulated MSCs were seeded in the upper chamber at a density of 8×10^4 cells, while fresh medium was supplied to the LPS-activated THP-1 cells in the lower chamber. After 48 h of co-culture, THP-1 cells were harvested for further analysis.

Flow cytometry analysis of THP-1 co-culture

THP-1 cells were seeded in a 6-well plate at a density of 3×10^5 cells per well and treated with 100 ng/mL

PMA for 48 h to induce differentiation into M0 macrophages. The culture medium was then replaced, and the cells were treated to 10 ng/mL LPS for an additional 48 h. After LPS treatment, MSCs or ITGA2 modulated MSCs were seeded in the upper chamber of a transwell insert at a density of 5×10^4 cells per well and co-culture for 24 h. Thereafter, the medium was refreshed, and the cells were incubated for an additional 96 h. After incubation, cells were washed with PBS and were harvested by treating each well with 1 mL of Accutase (Thermo Fisher Scientific) for 15 min at 37 °C. The cells were collected and centrifuged at 1200 rpm for 3 min at room temperature. The pellet was washed with FACS buffer (1% bovine serum albumin, 10% sodium azide, and 2 mM ethylenediaminetetraacetic acid) and then centrifuged. The pellet was resuspended in 100 μL of FACS buffer, and 5 μL of APC anti-human CD206 (MMR) Antibody (BioLegend, San Diego, CA, USA) was added. The samples were incubated on ice for 20 min. Following staining, the cells were washed twice with 1 mL of FACS buffer and then centrifuged. The cell pellet was resuspended in 100 µL of FACS buffer, and 5 µL of 7-AAD Viability Staining Solution (BioLegend) was added. The samples were incubated on ice for 10 min. Subsequently, 400 µL FACS buffer was added for further analysis. Flow cytometric analysis was performed using the Attune NxT Acoustic Focusing Cytometer (Invitrogen, Carlsbad, CA USA).

Statistical analysis

All data were expressed as the mean \pm standard error of the mean (SEM). Results were analyzed using unpaired t-test or two-way analysis of variance (ANOVA) and Tukey's method for multiple comparisons using the GraphPad Prism 9 software (GraphPad, Inc., La Jolla, CA, USA). P < 0.05, P < 0.01, P < 0.001, and P < 0.0001 (*, **, ***, and ****, respectively) were considered significant.

Results

Enhanced extracellular matrix (ECM) expression and adhesion-related transcripts in MSCs cultured in a 3D in vivo-mimicking microenvironment

Our previous studies demonstrated that culturing MSCs in a functional polymer-based 3D niche that mimics the in vivo microenvironment enhances their immunomodulatory and anti-inflammatory properties [25]. To further investigate the transcriptional changes underlying these functional enhancements, we performed RNA-seq transcriptome analysis comparing MSCs cultured under standard 2D conditions and a 3D in vivo-mimicking environment.

Principal Component Analysis (PCA) revealed a clear distinction between 3D and 2D MSCs, with minimal intra-group variance (Fig. 2A), indicating that the 3D microenvironment induces substantial transcriptional

Kang et al. Stem Cell Research & Therapy

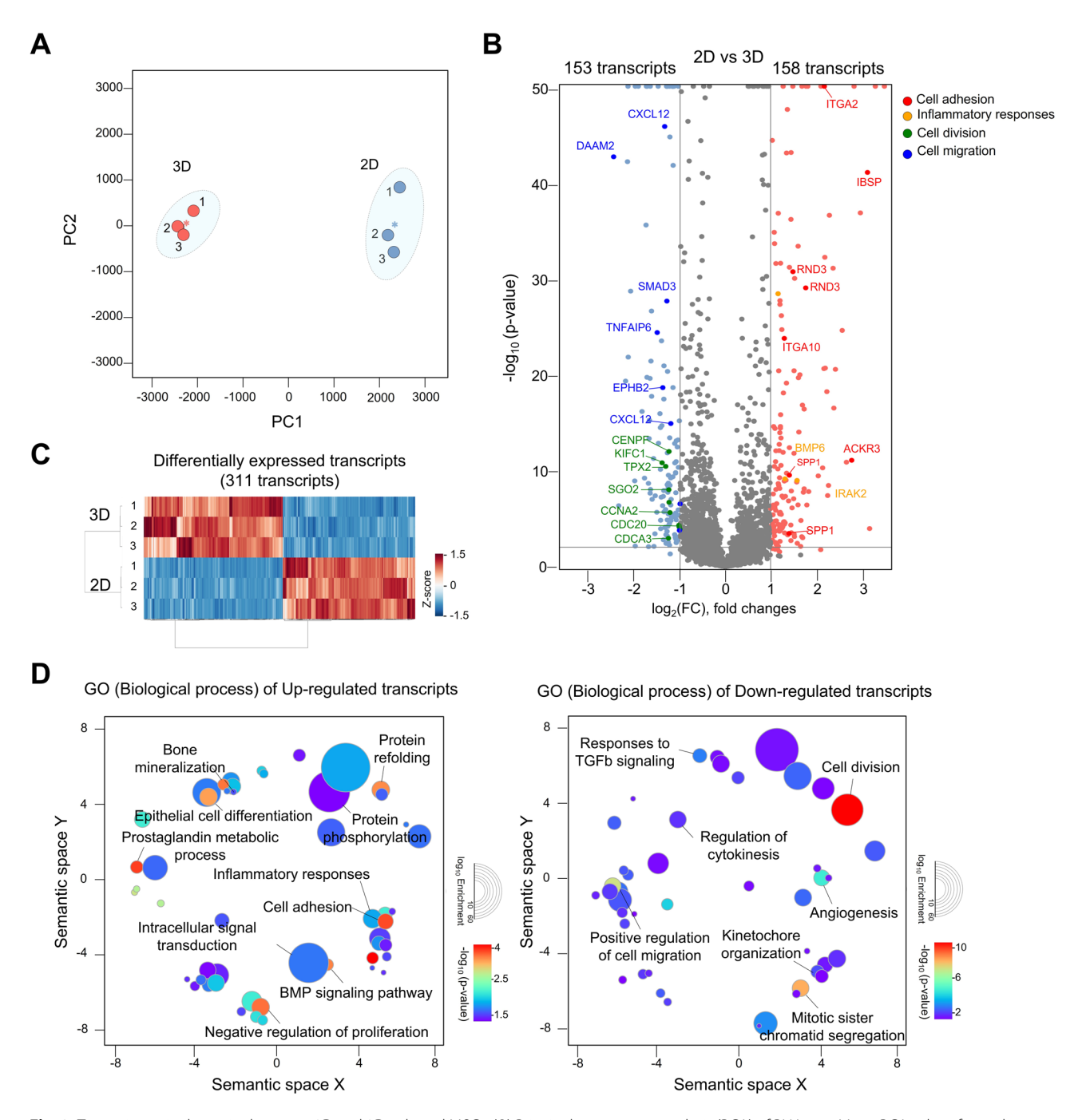


Fig. 2 Transcriptomic dynamics between 2D and 3D cultured MSCs. (**A**) Principal component analysis (PCA) of RNA-seq. Mean PCA values for each group are indicated as star marker. (**B**) Volcano plot illustrating the differential expression of transcripts (DETs) between MSCs cultured in 2D and 3D conditions. (**C**) Heatmap of RNA-seq analysis demonstrating differential transcript expression between 2D and 3D cultured MSCs. (**D**) The up- and downregulation of DETs between 2D and 3D cultured MSCs using Gene Ontology (GO) analysis

reprogramming in MSCs. This reprogramming leads to functionally distinct cellular states, confirming the validity of biological replicates (Fig. 2A, Supplementary Fig. 1). Volcano plot analysis (Fig. 2B) identified 158 upregulated and 153 downregulated transcripts, with upregulated genes related to 'cell adhesion' and 'inflammatory response', supporting the hypothesis that 3D

culture enhances cell-matrix interactions and immunomodulatory properties. In contrast, downregulated genes involved in 'cell division' and 'cell migration', suggesting a transition from a proliferative to a more specialized phenotype. Hierarchical clustering of differentially expressed transcripts (DETs) confirmed stable and reproducible transcriptional shifts (Fig. 2C).

Gene Ontology (GO) enrichment analysis (Fig. 2D) revealed upregulated pathways such as 'cell adhesion', 'inflammatory response', and 'negative regulation of proliferation, reinforcing the notion that MSCs in the 3D niche exhibit enhanced stability and immunomodulation. Additional pathways like 'BMP signaling', 'protein refolding, and 'epithelial cell differentiation' were enriched, indicating potential implications for tissue remodeling. Downregulated pathways were associated with 'cell division, 'TGF-β response,' 'cell migration,' and 'angiogenesis,' indicating a suppression of proliferative and migratory behaviors. Transcripts related to 'mitotic sister chromatid segregation' and 'cytokinesis regulation' were also significantly reduced, confirming the shift toward a guiescent, functionally optimized state. These findings suggest that 3D-cultured MSCs exhibit characteristics that enhance their engraftment, adhesion, and immunomodulation, which are crucial for improving MSC-based therapies for ALI/ARDS.

ITGA2 enhances MSC immunomodulatory function

Among the top differentially expressed genes, integrin alpha 2 (ITGA2) was significantly upregulated in 3D MSCs (Fig. 2B), as confirmed by qPCR and protein expression analyses (Supplementary Fig. 2A-B). To investigate the role of ITGA2 in MSC function, ITGA2 was

ectopically expressed in MSCs, leading to significantly increased PGE₂ secretion (Fig. 3A-B).

Co-culture with stimulated splenocytes demonstrated that ITGA2-MSCs suppressed TNF- α while upregulating IL-10 (Fig. 3C-D). Moreover, key immunoregulatory genes (*PTGS2*, *IDO*, *HMOX1*, and *PTGES*) were highly upregulated in ITGA2-MSCs, with IDO increasing by 1800-fold compared to that of the controls (Fig. 3E-H). These findings suggest that ITGA2 plays a crucial role in MSC-mediated immunosuppression.

ITGA2-MSCs attenuate ALI-induced inflammation

To assess ITGA2-MSC therapeutic potential, we used a murine LPS-induced ALI model. Blood IL-6 levels began to rise 1 h after ALI induction, peaked at 6 h, and then gradually declined by 24 h (Supplementary Fig. 3A). Based on this reference, intravenous administration of ITGA2-MSCs or control MSCs was performed 6 h after ALI induction, with blood and lung tissue samples collected at designated time points (Fig. 1A). IL-6 serum levels were measured to assess systemic inflammation. At 3 h post-LPS administration, inflammation levels were consistent across all groups, confirming model reliability (Fig. 1B). However, by 12 h, IL-6 levels in the ITGA2-MSC group were significantly lower than those in the vehicle and MSC groups (Fig. 1C), with further reductions observed at 24 h (Fig. 1D). Survival rates following

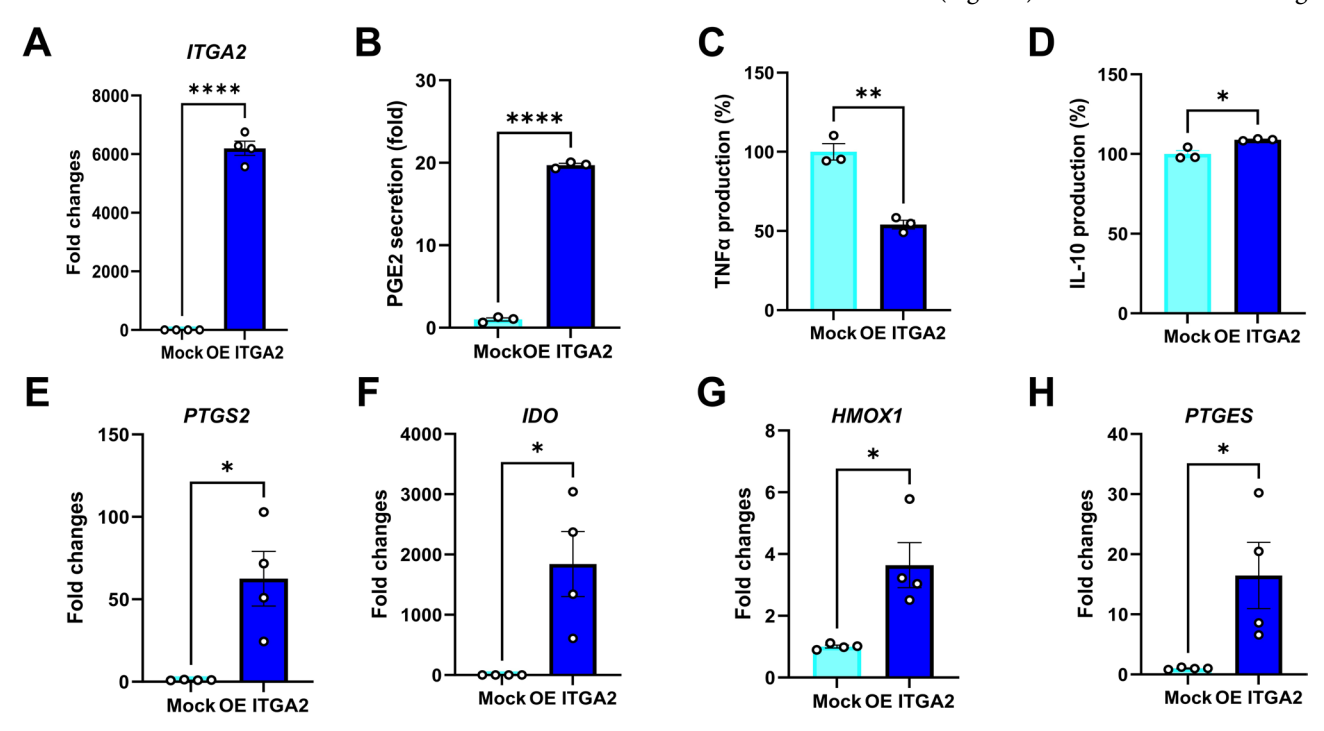


Fig. 3 ITGA2-MSCs enhance PGE_2 secretion and upregulate immunomodulatory factors. (**A**) qRT-PCR quantification of ITGA2 expression following transfection of MSCs with either mock or ITGA2 plasmid. (**B**) ELISA quantification of secreted PGE_2 in ITGA2-MSC culture supernatant. (**C**) and (**D**) ELISA analysis of TNF- α and IL-10 secretion in ITGA2-MSCs co-cultured with murine splenocytes (n=3). (**E-H**) Transcript levels of four genes classically identified as immunomodulatory factors, such as (**E**) PTGS2, (**F**) IDO, (**G**) HMOX1, and (**H**) PTGES, were measured in ITGA2-MSCs (n=4). Statistical significance was assessed using an unpaired t-test. *p < 0.05, **p < 0.01, ****p < 0.001

ALI and those of each cell-treated group were compared and presented using a Kaplan-Meier survival curve (Supplementary Fig. 3B).

Immunomodulatory factors (*PTGS2*, *NOS2*, *HMOX1*, and *IL10*) were also assessed. *PTGS2* and *HMOX1* were elevated in ALI but significantly reduced in ITGA2-MSC-treated mice (Fig. 1E-F). Moreover, iNOS levels were lower in ITGA2-MSCs than that in control MSCs at 24 h after ALI induction, suggesting a superior immunosuppressive effect (Fig. 1G). Additionally, anti-inflammatory effect of ITGA2-MSCs persisted by day 8 after ALI induction. As shown in Fig. 1H-J, the expression of *PTGS2* and its corresponding protein, COX2, were significantly reduced, along with a decrease in anti-inflammatory cytokine. Finally, IL-10 was elevated in ITGA2-MSC group, indicating the sustained anti-inflammatory effect of ITGA2-MSCs.

ITGA2-MSCs exhibit enhanced in vivo survival and adaptation

ITGA2-MSCs exhibited a sustained anti-inflammatory and immunomodulatory effect. To assess whether ITGA2 improves MSC engraftment, IVIS was used over a 7-day period following intravenous administration.

ITGA2-MSCs exhibited significantly higher fluorescence intensity than control MSCs, with peak retention between days 2–3, followed by gradual decline (Fig. 4A-B). Notably, tissue biodistribution analysis showed enhanced retention in the lungs, liver, and spleen, suggesting improved survival and adaptation in vivo (Fig. 4C).

ITGA2-MSCs promote lung tissue repair and immune modulation

Histopathological examination of lung tissue 8 days post-ALI induction revealed severe lung edema and inflammatory cell infiltration in the vehicle group, whereas MSC and ITGA2-MSC groups exhibited significantly reduced damage (Fig. 5A). ALI severity scoring confirmed substantial improvements in the ITGA2-MSC group compared to both the vehicle and MSC groups (Fig. 5B). Notably, ITGA2-MSC administration not only improved lung fibrosis, indicative of fixed tissue injury, but also significantly enhanced respiratory function in ALI animals (Supplementary Fig. 4A and B).

To further assess lung barrier integrity, we analyzed the expression of tight junction markers (*OCLN*, *CLDN2*, and *CLDN4*). *OCLN*, associated with lung barrier

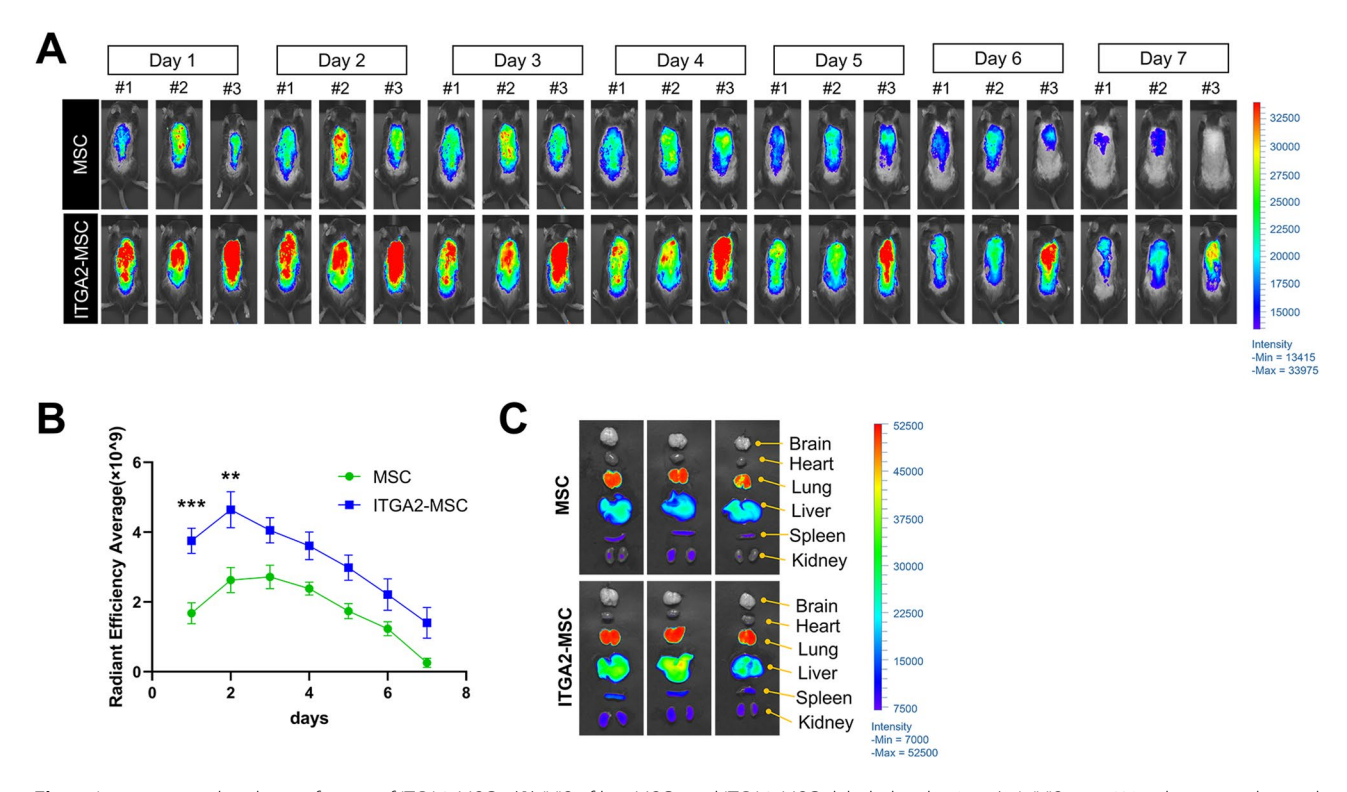


Fig. 4 In vivo survival and engraftment of ITGA2-MSCs. (**A**) IVIS of live MSCs and ITGA2-MSCs labeled with 50 μg/mL IVISense 680, administered via tail vein injection, and tracked up to day 7. Pseudo-color intensity scale: red (highest) to blue (lowest) (**B**) Quantitative fluorescence analysis over 7 days (n = 3 per group). The fluorescence intensity within the region of interest (ROI) was quantitatively compared over time between MSCs and ITGA2-MSCs. (**C**) Ex vivo fluorescence imaging of brain, heart, lungs, liver, spleen, and kidneys on day 7 post-injection, demonstrating differential biodistribution of ITGA2-MSCs. Data were expressed as mean ± standard error of the mean (SEM), and statistical significance was determined using two-way ANOVA. **p<0.01, ***p<0.001

Kang et al. Stem Cell Research & Therapy

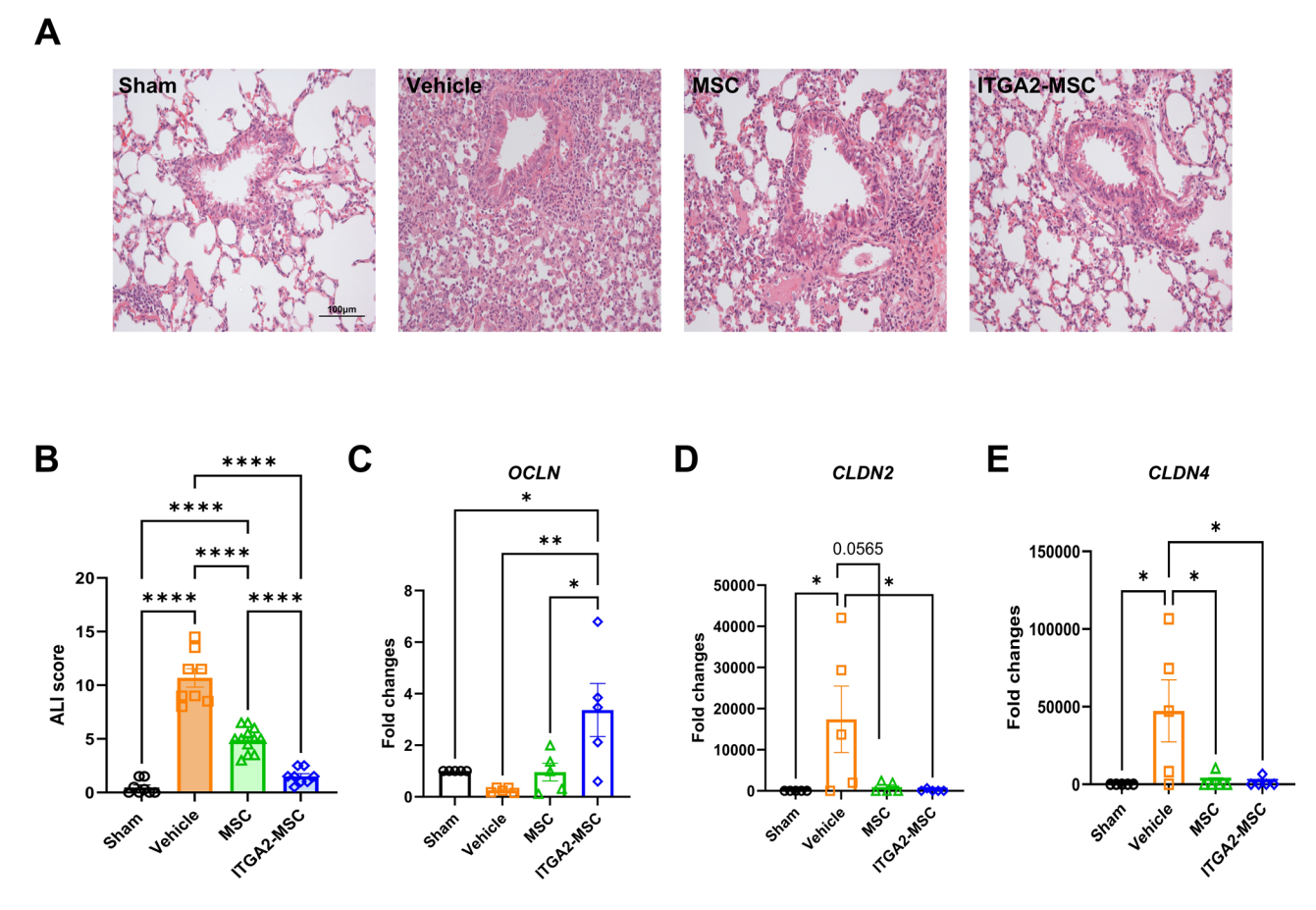


Fig. 5 Histological and molecular analysis of ITGA2-MSC-mediated lung protection. (**A**) Representative H&E-stained lung tissue sections from ALI mice 8 days post-injection. Scale bar = $100 \mu m$. (**B**) ALI severity scoring across experimental groups (n=8-11 per group). (**C-E**) Transcript levels of three genes related to tight junction such as *OCLN*, *CLDN2*, and *CLDN4* in lung tissues (n=5 per group). Statistical significance was determined using two-way ANOVA. *p < 0.005, **p < 0.01, *****p < 0.001

function, was significantly increased in the ITGA2-MSC group, whereas *CLDN2* and *CLDN4*, markers of lung edema, were reduced (Fig. 5C-E). These findings suggest that ITGA2-MSCs not only reduce lung inflammation but also promote epithelial barrier recovery in ALI.

ITGA2-MSCs induce M2 macrophage polarization in ALI mouse lungs

Given the observed suppression of TNF- α and IL-6 along with the elevation of IL-10 (Figs. 1 and 3), we investigated whether ITGA2-MSCs facilitated M2 macrophage polarization in the lung. Immunofluorescence staining for CD206 as M2 marker showed a pronounced increase in the ITGA2-MSC group (Fig. 6A). Transcriptional analysis further revealed reduced M1 macrophage markers (*NOS2*), although CD86 was not significantly changed (Fig. 6B). Further ITGA2-MSC group markedly elevated M2 markers (*CD206*, *ARG1*) compared to vehicle or MSC group (Fig. 6C), indicating a shift from M1 to M2 polarization by day 8.

Mechanisms underlying ITGA2-MSC therapeutic action via M2 macrophage polarization

To determine whether ITGA2-MSCs directly induce M2 macrophage polarization, we performed in vitro co-culture assays using a transwell system. Before inducing macrophage polarization, THP-1 monocytes were treated with PMA to promote their differentiation into M0 macrophage (Fig. 7A). Control MSCs or ITGA2-MSC were cultured in the upper chamber, while PMA-treated THP-1 cells were maintained in the lower chamber for indirect co-culture (Fig. 7B). Consistent with our in vivo findings, gene expression analysis revealed a decrease in the M1 marker CD86 and an increase in the M2 marker CD206 in THP-1 cells co-cultured with ITGA2-MSCs (Fig. 7C). Although IL-10 expression was slightly enhanced in ITGA2-MSC co-cultures, it was not statistically significant. Finally, flow cytometry confirmed increased CD206 surface expression in THP-1 macrophages after co-culture with MSCs or ITGA2-MSCs. Dot plot analysis demonstrated an increase in CD206 expression in the ITGA2-MSC group, and the mean

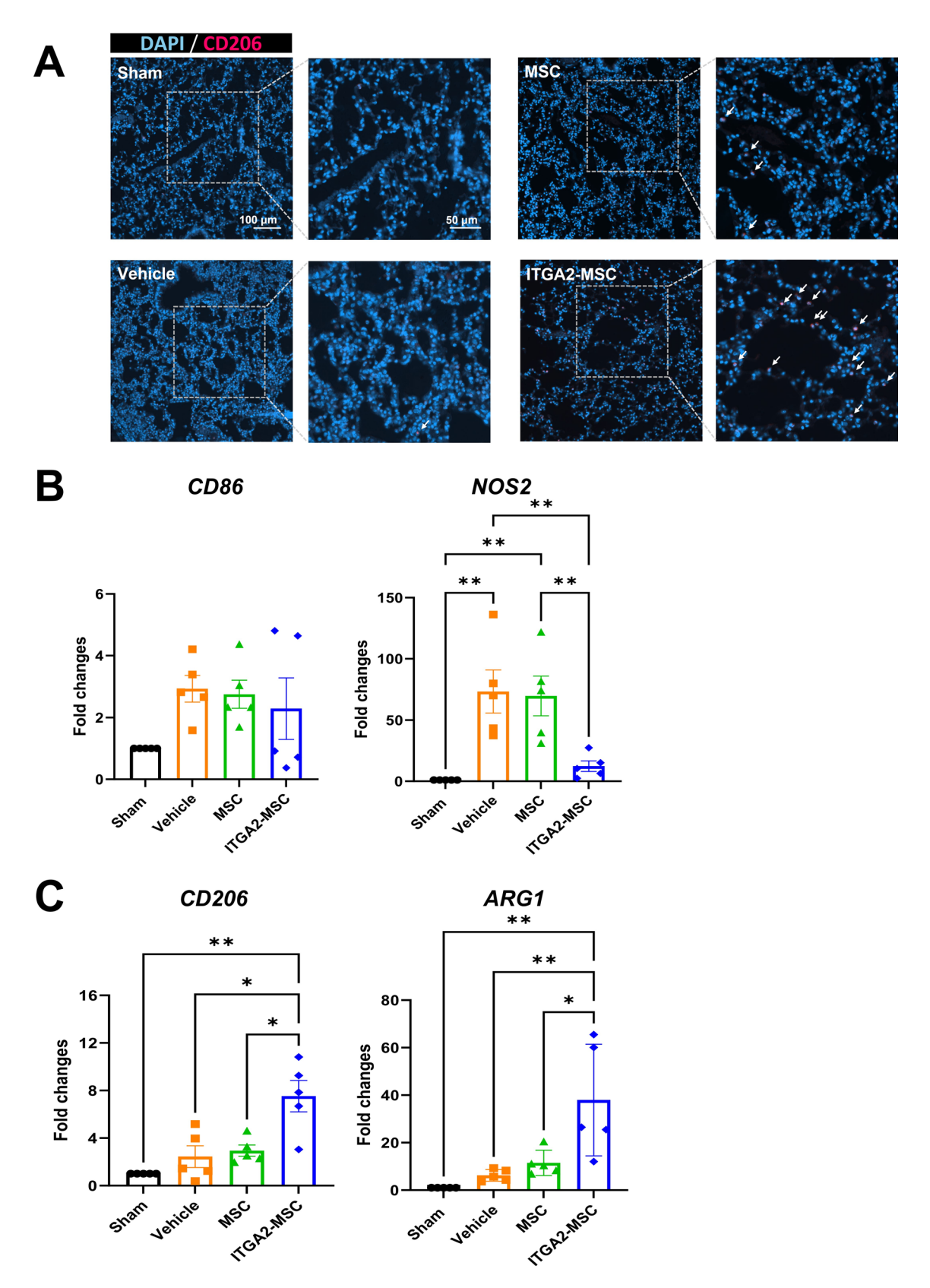


Fig. 6 ITGA2-MSCs promote M2 macrophage polarization in ALI mouse lungs. (**A**) Representative immunofluorescence staining of lung sections at day 8 post-LPS injection. CD206+macrophages (red) were visualized using anti-CD206 antibody, and nuclei were counterstained with DAPI (blue). White arrows indicate CD206+cells. Scale bars = $100 \mu m$, $50 \mu m$. (**B-C**) Transcript level of M1 macrophage markers (*CD86*, *NOS2*) and M2 macrophage markers (*CD206*, *ARG1*) in lung tissues ($n = 5 \mu m$). Statistical significance was determined using two-way ANOVA. *p < 0.05, **p < 0.05, **p < 0.01

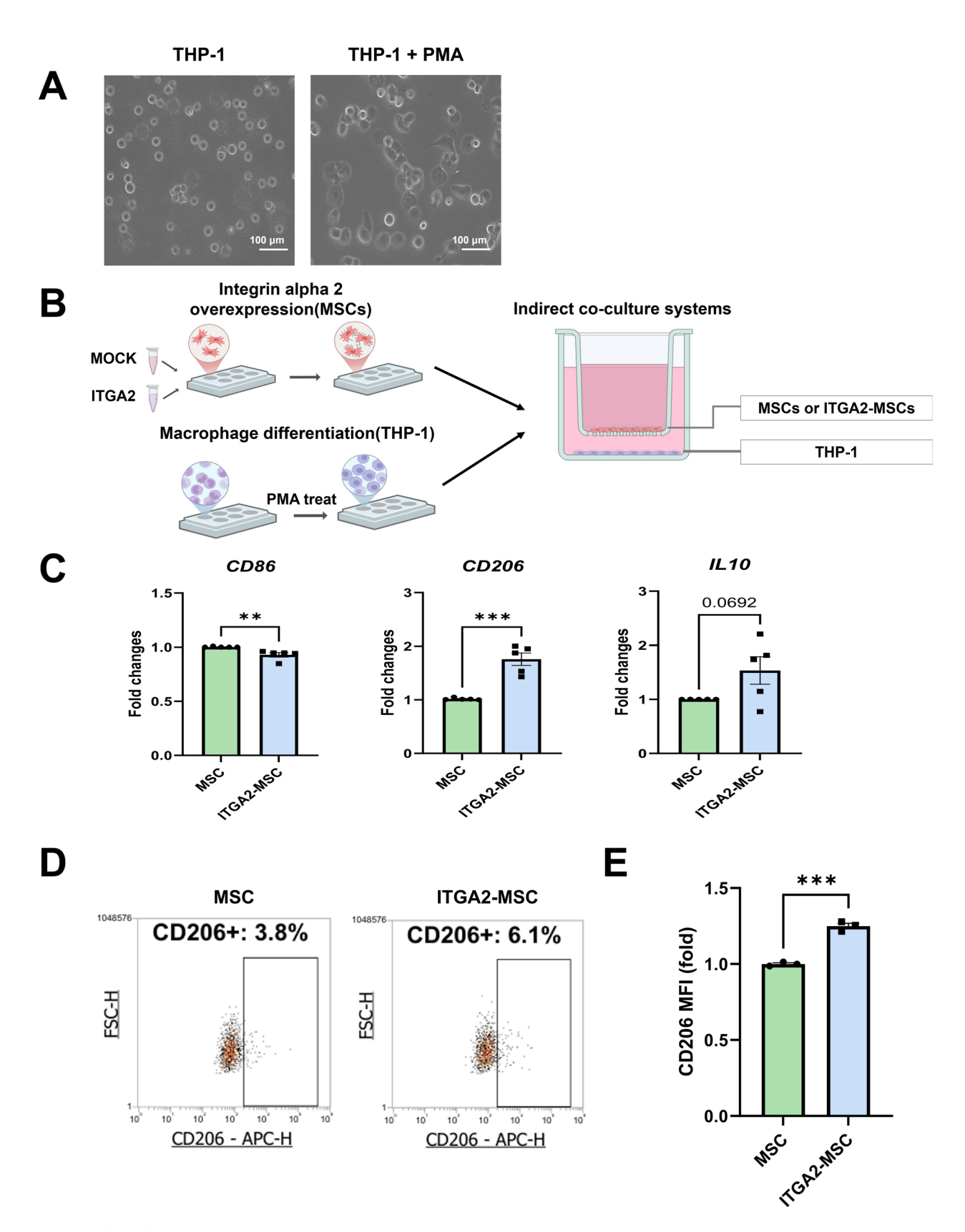


Fig. 7 (See legend on next page.)

(See figure on previous page.)

Fig. 7 ITGA2-MSCs modulate macrophage polarization. (**A**) Representative phase-contrast microscopy images showing morphological changes in THP-1 cells with or without PMA treatment for 24 h. (**B**) Schematic representation of the co-culture system for PMA-differentiated THP-1 macrophages and MSCs or ITGA2-MSCs. (**C**) qRT-PCR analysis of macrophage phenotype markers in THP-1 cells after 48 h co-culture. *CD86*, *CD206*, and *IL10* expression levels were normalized to GAPDH (n=5). (**D**) Flow cytometry analysis of CD206 expression on THP-1 macrophages, and (**E**) the quantification graph. Three independent experiments were repeated (n=3). Statistical analysis was performed using an unpaired t-test. **p<0.001

fluorescence intensity (MFI) values were used for relative quantification (Fig. 7D-E). Overall, these findings suggest that ITGA2-MSCs enhance MSC immunomodulatory functions, improve survival, and potentiate therapeutic effects in ALI by inducing M2 macrophage polarization.

Discussion

Our RNA-seq analysis revealed that culturing MSCs in a niche-mimicking 3D platform significantly upregulated the expression of adhesion-related molecules, including ITGA2, compared to traditional 2D MSC cultures. This upregulation is particularly relevant, as integrins play a pivotal role in MSC adhesion, survival, and function. Furthermore, ectopic expression of ITGA2 in MSCs enhanced immunomodulatory and anti-inflammatory gene expression, leading to significant improvement in lung repair in an ALI model.

Beyond molecular expression profiles, the intravenous administration of ITGA2-MSCs resulted in prolonged survival and improved adaptation in vivo. Notably, ITGA2-MSCs directly promoted macrophage polarization toward the M2 phenotype, a hallmark of anti-inflammatory and tissue-reparative macrophages. These findings suggest that ITGA2-primed MSCs possess enhanced regenerative potential, reinforcing their therapeutic efficacy in both tissue repair and immune modulation.

Mechanistically, ITGA2 overexpression in MSCs modulated key immunoregulatory pathways (Fig. 3). Among them, *PTGS2* and *HMOX1*—both inducible by inflammatory stimuli—were significantly upregulated in ITGA2-MSCs, contributing to the resolution of inflammation. *PTGS2* encodes COX-2, the rate-limiting enzyme in prostaglandin E2 (PGE₂) synthesis, and its upregulation correlated with increased PGE₂ production (Fig. 3B, E). In the ALI model, *PTGS2* and *HMOX1* expression levels were modestly elevated in the ITGA2-MSC group compare to the vehicle and non-modified MSC groups (Fig. 1E, G, H), indicating that ITGA2-MSCs foster a controlled inflammatory environment rather than provoking excessive immune activation. This moderate response likely reflects an adaptive immunomodulatory mechanism

Integrins are central to MSC adhesion, migration, and immune interactions [28–30]. MSCs express various integrin heterodimers that enable binding to extracellular matrix (ECM) components such as fibronectin, collagen, and laminins [31]. These adhesion properties are

essential for MSCs delivered systemically, facilitating their vascular transit, tissue extravasation, and homing to injury sites [32–36]. Indeed, ITGA2 and ITGA10—both known to be expressed in MSCs [37]—were significantly upregulated under 3D culture conditions (Fig. 2B), despite their low basal expression in 2D-cultured MSCs (Supplementary Fig. 5). While this study highlights the therapeutic potential of ITGA2-engineered MSCs, further investigation is warranted to elucidate the roles of other integrins, such as ITGA10 and ITGA4. These integrins are known to bind collagen within the extracellular matrix and, in association with integrin b1, contribute to MSC proliferation and migration [38, 39].

The functional relevance of integrin subtype specificity in MSC biology is well documented. For example, Clark et al. demonstrated that synthetic peptides targeting the α2β1 integrin significantly altered MSC cytokine secretion profiles, indicating that integrin subtype specificity influences MSC-mediated immune modulation [39]. In parallel, ITGA4-overexpressing MSCs exhibited enhanced cerebral homing following intracarotid transplantation in a stroke model, reducing cell aggregation and embolic risk [40]. Additionally, CD47—a known as integrin-associated protein—mediated MSC-induced immune regulation through the Hedgehog/SMO/Gli1 signaling pathway in a liver inflammation model [41], further underscoring the integrin-dependent mechanisms underlying MSC immunoregulatory functions.

Our study extends this understanding by demonstrating that ITGA2-overexpressing MSCs exhibit prolonged survival and improved in vivo adaptation compared to control MSCs (Fig. 4A, B). IVIS imaging confirmed that ITGA2-MSCs maintained the highest fluorescence intensity for up to three days post-injection, gradually declining by day 7. Furthermore, tissue biodistribution analysis revealed increased retention of ITGA2-MSCs in the lung, liver, and spleen, suggesting enhanced engraftment and survival post-transplantation (Fig. 4C). These findings reinforce the hypothesis that modulating integrin expression, particularly ITGA2, enhances MSC homing efficiency and therapeutic efficacy in tissue repair and immune modulation.

Intravenously administered MSCs are predominantly short-lived, with most being sequestered in the lungs within one hour post-infusion [42]. This transient lung retention suggests that MSCs may be particularly effective in modulating inflammation in pulmonary injuries such as ALI and ARDS [43, 44]. Consistently,

ITGA2-MSCs not only exhibited prolonged in vivo survival but also actively promoted M2 macrophage polarization (Fig. 6A). Furthermore, ITGA2-MSC administration enhanced tight junction markers in the injured lung, suggesting that ITGA2 expression supports both macrophage-mediated immune modulation and lung barrier restoration.

Our in vitro co-culture assays further confirmed that ITGA2-MSCs directly upregulated CD206 expression on macrophages, promoting M2 macrophage polarization (Fig. 6B-D). While the precise molecular mechanism underlying ITGA2-mediated macrophage polarization remains unclear, our RNA-seq data revealed enhanced BMP signaling (Fig. 2). Given that Smad-mediated BMP signaling has been previously implicated in promoting M2 polarization [45], it is plausible that ITGA2 may engage this pathway to modulate macrophage phenotype. Additionally, as MSC-derived exosome are known to contribute to M2 polarization and immune regulation [46-49], future studies should explore whether ITGA2 expression enhances exosome biogenesis or cargo composition, thereby augmenting macrophage reprogramming through paracrine mechanisms.

This study employed a single dose of ITGA2-MSCs administered six hours after ALI induction, with in vivo persistence detectable for up to 7 days. However, further dose-response studies and extended tracking periods are necessary to determine the optimal and minimally effective therapeutic dose for potential clinical applications.

Additionally, only male mice were used in this study. Given that some reports [50] have indicated sex-based differences in inflammatory responses and the efficacy of cell-based therapies, future studies should consider including both sexes to better inform translational relevance. Moreover, further investigation into the key molecular mediators—such as small molecules or regulatory RNAs—underlying ITGA2-MSC-mediated immune modulation will provide deeper mechanistic insights. Understanding these mediators will not only advance MSC-based therapies but also inform potential combination strategies with pharmacological agents to enhance therapeutic outcomes.

Conclusions

We demonstrated that the ectopic expression of the adhesion molecule ITGA2 in MSCs enhanced immunomodulatory gene expression and promoted M2 macrophage polarization in an ALI model. Notably, ITGA2-MSCs exhibited significantly improved cellular adaptation and retention in vivo following intravenous administration compared to control MSCs, suggesting that ITGA2-engineered MSCs could enhance cell survival and adaptation efficiency in cell therapy. While further evaluation is needed to determine the optimal dosage and duration of

MSC administration for maximum therapeutic efficacy, our findings highlight the potential of adhesion molecule-primed MSCs as a promising strategy for regenerative medicine.

Abbreviations

ALI Acute lung injury
MSCs Mesenchymal stromal cell

ITGA Integrin alpha
ARDS Acute respiratory distress syndrome

ICU Intensive care unit
IL Interleukin
RNA-seq RNA sequencing
LPS Lipopolysaccharide
RT Room temperature

qRT-PCR Quantitative real-time polymerase chain reaction

TBS Tris- buffered saline COX-2 Cyclooxygenase-2

iNOS Inducible nitric oxide synthase
NBF Neutral buffered formalin
IVIS In vivo imaging system
PBS Phosphate buffered saline
TNF-a Tumor necrosis factor-a
GO Gene ontology
COX2 Cyclooxygenase-2

HO1 Heme oxygenase 1 PGE2 Prostaglandin E2

PTGS2 Prostaglandin-endoperoxide synthase 2

PTGES Prostaglandin E synthase
IDO Indoleamine 2,3-dioxygenase
HMOX1 Heme oxygenase 1 gene

OCLN Occludin
CLDN2 Claudin 2
CLDN4 Claudin 4
ARG1 Arginase 1

Supplementary Information

The online version contains supplementary material available at https://doi.org/10.1186/s13287-025-04423-1.

Supplementary Material 1

Acknowledgements

The authors declare that they have not use Al-generated work in this manuscript.

Author contributions

HK performed all the experiments. OHK, JK, JYK, GSS, CHK and JWK contributed to RNAseq experiment and analysis. OHK and ESC contributed to biochemical analysis. YL contributed to flow cytometry experiment and analysis. HK, OHK, YJS, JWK and HJL contributed to the manuscript writing, reviewing and editing. HJL contributed to the conception, design, financial support. All authors were involved in the final approval of the manuscript.

Funding

This work was financially supported by a National Research Foundation of Korea (NRF) grant funded by the Korean government (Grant Nos.2023R1A2C2006894, RS-2024-00409554, RS-2023-00220089, 2023R1A2C1007657 and RS-2024-00361192).

Data availability

All data analyzed during this study are included in this published article and its supplementary information file. The dataset used in Fig. 2 and supplementary information are downloaded from Gene Expression Omnibus (GEO) database under accession number GSE236113.

Declarations

Ethics approval and consent to participate

The study was reviewed and approved by the IACUC of Chung-Ang University (Approval ID: 202301020051) as follows; (1) Title of the approved project: Validation of septic shock treatment with preconditioned MSCs (2) Name of the institutional approval committee: IACUC of Chung-Ang University (3) Approval number: 202301020051 (4) Date of approval: June 21, 2023. Human MSCs were purchased from AllCells, which has confirmed that the initial collection of the cells was conducted with ethical approval and that informed consent was obtained from all donors. The human THP-1 cell line was purchased from the Korean Cell Line Bank and was originally established in 1980. We have cited the original publication and submitted the certificate of analysis (COA) for reference.

Consent for publication

Not applicable.

Competing interests

The authors have declared that they have no competing interests.

Author details

¹Department of Global Innovative Drugs, Graduate School of Chung-Ang University, Seoul 06974, South Korea

²Department of Anatomy and Cell Biology, College of Medicine, Chung-Ang University, Seoul 06974, South Korea ³Department of Life Science, Chung-Ang University, Seoul 06974, South Korea

Received: 19 March 2025 / Accepted: 26 May 2025 Published online: 03 June 2025

References

- Matthay MA, et al. Acute respiratory distress syndrome. Nat Rev Dis Primers. 2019-5(1):18
- 2. Hussain M, et al. Acute respiratory distress syndrome and COVID-19: A literature review. J Inflamm Res. 2021;14:7225–42.
- Tzotzos SJ, et al. Incidence of ARDS and outcomes in hospitalized patients with COVID-19: a global literature survey. Crit Care. 2020;24(1):516.
- Bellani G, et al. Epidemiology, patterns of care, and mortality for patients with acute respiratory distress syndrome in intensive care units in 50 countries. JAMA. 2016;315(8):788–800.
- Palakshappa JA, et al. Long-Term outcomes in acute respiratory distress syndrome: epidemiology, mechanisms, and patient evaluation. Crit Care Clin. 2021;37(4):895–911.
- Mart MF, Ware LB. The long-lasting effects of the acute respiratory distress syndrome. Expert Rev Respir Med. 2020;14(6):577–86.
- Spragg RG, et al. Beyond mortality: future clinical research in acute lung injury. Am J Respir Crit Care Med. 2010;181(10):1121–7.
- Luo Y, et al. Overexpression of FoxM1 optimizes the therapeutic effect of bone marrow mesenchymal stem cells on acute respiratory distress syndrome. Stem Cell Res Ther. 2023;14(1):27.
- Hezam K, et al. Superior protective effects of PGE2 priming mesenchymal stem cells against LPS-induced acute lung injury (ALI) through macrophage Immunomodulation. Stem Cell Res Ther. 2023;14(1):48.
- Cao JP, et al. Autologous transplantation of peripheral blood-derived Circulating endothelial progenitor cells attenuates endotoxin-induced acute lung injury in rabbits by direct endothelial repair and indirect Immunomodulation. Anesthesiology. 2012;116(6):1278–87.
- 11. Guillamat-Prats R et al. Alveolar type II cells or mesenchymal stem cells: comparison of two different cell therapies for the treatment of acute lung injury in rats. Cells, 2020;9(8).
- 12. Lee JW, et al. Concise review: mesenchymal stem cells for acute lung injury: role of paracrine soluble factors. Stem Cells. 2011;29(6):913–9.
- Si YL, et al. MSCs: biological characteristics, clinical applications and their outstanding concerns. Ageing Res Rev. 2011;10(1):93–103.
- Muller L, et al. Immunomodulatory properties of mesenchymal stromal cells: an update. Front Cell Dev Biol. 2021;9:637725.
- Ma S, et al. Immunobiology of mesenchymal stem cells. Cell Death Differ. 2014;21(2):216–25.

- Nemeth K, et al. Bone marrow stromal cells attenuate sepsis via prostaglandin E(2)-dependent reprogramming of host macrophages to increase their interleukin-10 production. Nat Med. 2009;15(1):42–9.
- 17. Lee JW, et al. Allogeneic human mesenchymal stem cells for treatment of E. coli endotoxin-induced acute lung injury in the ex vivo perfused human lung. Proc Natl Acad Sci U S A. 2009;106(38):16357–62.
- Matthay MA, et al. Treatment with allogeneic mesenchymal stromal cells for moderate to severe acute respiratory distress syndrome (START study): a randomised phase 2a safety trial. Lancet Respir Med. 2019;7(2):154–62.
- Bellingan G et al. Primary Analysis of a Phase 1/2 Study to Assess MultiStem[®] Cell Therapy, a Regenerative Advanced Therapy Medicinal Product (ATMP), in Acute Respiratory Distress Syndrome (MUST-ARDS). Am J Respir Crit Care Med, 2019;199:A7353–A7353.
- Zheng G, et al. Treatment of acute respiratory distress syndrome with allogeneic adipose-derived mesenchymal stem cells: a randomized, placebocontrolled pilot study. Respir Res. 2014;15(1):39.
- Liu C, Xiao K, Xie L. Advances in mesenchymal stromal cell therapy for acute lung injury/acute respiratory distress syndrome. Front Cell Dev Biol. 2022;10:951764.
- 22. Turner NJ, et al. Alpha2(VIII) collagen substrata enhance endothelial cell retention under acute shear stress flow via an alpha2beta1 integrin-dependent mechanism: an in vitro and in vivo study. Circulation. 2006;114(8):820–9.
- 23. Liu S et al. Integrin alpha2beta1 regulates collagen I tethering to modulate hyperresponsiveness in reactive airway disease models. J Clin Invest, 2021;131(12).
- 24. Wang S, et al. Excess integrins cause lung entrapment of mesenchymal stem cells. Stem Cells. 2015;33(11):3315–26.
- Kim OH, et al. Extended protective effects of three dimensional cultured human mesenchymal stromal cells in a neuroinflammation model. World J Stem Cells. 2025;17(1):101485.
- 26. Tsuchiya S, et al. Establishment and characterization of a human acute monocytic leukemia cell line (THP-1). Int J Cancer. 1980;26(2):171–6.
- 27. Matute-Bello G, et al. An official American thoracic society workshop report: features and measurements of experimental acute lung injury in animals. Am J Respir Cell Mol Biol. 2011;44(5):725–38.
- Hynes RO. Integrins: bidirectional, allosteric signaling machines. Cell. 2002;110(6):673–87.
- Guilak F, et al. Control of stem cell fate by physical interactions with the extracellular matrix. Cell Stem Cell. 2009;5(1):17–26.
- Parsons JT, Horwitz AR, Schwartz MA. Cell adhesion: integrating cytoskeletal dynamics and cellular tension. Nat Rev Mol Cell Biol. 2010;11(9):633–43.
- Gronthos S, et al. Integrin-mediated interactions between human bone marrow stromal precursor cells and the extracellular matrix. Bone. 2001;28(2):174–81.
- 32. Ullah M, Liu DD, Thakor AS. Mesenchymal Stromal Cell Homing: Mech Strategies Improv iScience. 2019;15:421–38.
- Hu HJ, et al. Integrin beta 3-overexpressing mesenchymal stromal cells display enhanced homing and can reduce atherosclerotic plaque. World J Stem Cells. 2023;15(9):931–46.
- Popov C, et al. Integrins alpha2beta1 and alpha11beta1 regulate the survival of mesenchymal stem cells on collagen I. Cell Death Dis. 2011;2(7):e186.
- Clark AY, et al. Integrin-specific hydrogels modulate transplanted human bone marrow-derived mesenchymal stem cell survival, engraftment, and reparative activities. Nat Commun. 2020;11(1):114.
- Steingen C, et al. Characterization of key mechanisms in transmigration and invasion of mesenchymal stem cells. J Mol Cell Cardiol. 2008;44(6):1072–84.
- 37. Pang X, et al. Targeting integrin pathways: mechanisms and advances in therapy. Signal Transduct Target Ther. 2023;8(1):1.
- Edstrom D, et al. Integrin alpha10beta1-selected mesenchymal stem cells reduced hypercoagulopathy in a Porcine model of acute respiratory distress syndrome. Respir Res. 2023;24(1):145.
- 39. Martino MM, et al. Controlling integrin specificity and stem cell differentiation in 2D and 3D environments through regulation of fibronectin domain stability. Biomaterials. 2009;30(6):1089–97.
- Cui LL, et al. Integrin alpha4 overexpression on rat mesenchymal stem cells enhances transmigration and reduces cerebral embolism after intracarotid injection. Stroke. 2017;48(10):2895–900.
- Sheng M, et al. CD47-Mediated Hedgehog/SMO/GL11 signaling promotes mesenchymal stem cell Immunomodulation in mouse liver inflammation. Hepatology. 2021;74(3):1560–77.

- 42. Eggenhofer E, et al. Mesenchymal stem cells are short-lived and do not migrate beyond the lungs after intravenous infusion. Front Immunol. 2012;3:297.
- 43. Zhang X, et al. Mesenchymal stromal cells alleviate acute respiratory distress syndrome through the cholinergic anti-inflammatory pathway. Signal Transduct Target Ther. 2022;7(1):307.
- 44. Golmohammadi M, et al. Human fetal lung mesenchymal stem cells ameliorate lung injury in an animal model. Sci Rep. 2025;15(1):6433.
- Rocher C, Singla DK. SMAD-PI3K-Akt-mTOR pathway mediates BMP-7 polarization of monocytes into M2 macrophages. PLoS ONE. 2013;8(12):e84009.
- 46. Arabpour M, Saghazadeh A, Rezaei N. Anti-inflammatory and M2 macrophage polarization-promoting effect of mesenchymal stem cell-derived exosomes. Int Immunopharmacol. 2021;97:107823.
- Lo Sicco C, et al. Mesenchymal stem Cell-Derived extracellular vesicles as mediators of Anti-Inflammatory effects: endorsement of macrophage polarization. Stem Cells Transl Med. 2017;6(3):1018–28.

- Teo KYW et al. Mesenchymal Stromal Cell Exosomes Mediate M2-like Macrophage Polarization through CD73/Ecto-5'-Nucleotidase Activity. Pharmaceutics, 2023;15(5).
- 49. He X, et al. MSC-Derived exosome promotes M2 polarization and enhances cutaneous wound healing. Stem Cells Int. 2019;2019:p7132708.
- Shen H, et al. Sex differences in the therapeutic effect of unaltered versus NFkappaB sensing IL-4 over-expressing mesenchymal stromal cells in a murine model of chronic inflammatory bone loss. Front Bioeng Biotechnol. 2022;10:962114.

Publisher's note

Springer Nature remains neutral with regard to jurisdictional claims in published maps and institutional affiliations.